Application of a surface-consistent matching filters (SCMF) on a time-lapse data set

Mahdi Almutlaq and Gary F. Margrave

ABSTRACT

This paper presents a new idea for designing a matching filter for processing time-lapse seismic data in a surface-consistent manner. We extend the surface-consistent data model to the case of designing matching filters to equalize two seismic surveys in the least-squares sense. The frequency-domain surface-consistent design equations are similar to those for surface-consistent deconvolution except that the data term is the spectral ratio of two surveys. Since taking spectral ratios poses a challenge, we design the matching filters in a least-squares sense in the time domain and Fourier transform the result. We decompose the result into four surface-consistent components: source, receiver, offset, and midpoint. Each of these components collects unique effects thus providing us with freedom on how to utilize them.

We discuss two examples that demonstrate how the matching filters are constructed and implemented. In the first example, we apply all four-components to the first monitoring survey to match it to the baseline survey, whose subsurface (the reservoir) is unchanging but shows surface-consistent variability. In the operator window, the residual between the matched survey and the baseline survey is extremely small.

The second example is between first monitoring survey and second monitoring survey where the reservoir is variable and shows surface-consistent variability as well. In this case, the residual is close to zero in the matching filter window.

INTRODUCTION

It has become an industry practice to acquire multiple seismic surveys at certain time intervals to monitor subsurface changes due to hydrocarbon production or fluid injection. As exploration seismologists, our main goal is to obtain an image that represents our best estimate of the subsurface. But we know from the many years of experience that this goal is difficult to achieve due to inconsistency in recording instruments, conditions on the earth's surface (in the case of land data) and the many undesired variations added to our recorded seismic wavelet. These problems, among many others summarized by Jack (1998), are known as the cause of the nonrepeatability of time-lapse seismic survey. Despite this painful fact, we focus our resources on minimizing the previously mentioned effects to produce our best estimate image of the subsurface.

In this paper, we first review our innovative approach introduced in last year's report by Almutlaq and Margrave (2010) that described the design of a surface-consistent matching filters. We briefly introduce the background followed by constructing a theoretical framework of this new concept. We support our theoretical claim by presenting two synthetic examples that exhibit how this new filtering technique reduce to a great extent the nonrepeatability issue of time-lapse seismic survey.

A review of the surface-consistent model

Taner and Coburn (1980) were first to suggest that the recorded seismic trace can be modeled as the convolution of each trace's source effect, receiver effect, offset effect and midpoint effect. This four-component model is known as the surface-consistent model. It is similar to that used by Taner et al. (1974) and Wiggins et al. (1976) for solving the statics problem. Many other authors have implemented this model in obtaining a more accurate and stable deconvolution (Morley and Claerbout, 1983; Levin, 1989; Cambois and Stoffa, 1992; Cary and Lorentz, 1993), amplitude balancing (Yu, 1985), and phase-rotation problem (Taner et al., 1991).

There are two classes of surface-consistent effects. The first one is related to the surface and the second is related to the subsurface and are classified as follow (Taner and Koehler, 1981):

1. $s_i(t)$: Source response at surface location i. This term contains the near-surface effects imposed on the downgoing source waveform.

2. $r_j(t)$: Receiver response at surface location j. This term contains the near-surface influence on the recorded waveform.

3. $h_k(t)$: Offset response at offset location k, where $k = |i - j|$. This contains offset related effects such as spherical divergence or residual moveout.

4. $y_l(t)$: Subsurface response below surface location l. This contains the response of all traces with common midpoint $l = \frac{(i+j)}{2}$.

Taner and Koehler (1981) and Morley and Claerbout (1983) modeled the seismic trace as the convolution of four operators:

$$d_{ij}(t) = s_i(t) * r_j(t) * h_k(t) * y_l(t) \tag{1}$$

where $d_{ij}(t)$ represents the seismic trace and the asterisk ($*$) denotes the convolution in time domain, t.

Estimating the four-components ($s_i(t)$, $r_j(t)$, $h_k(t)$, and $y_l(t)$) from the seismic trace is known as surface-consistent decomposition (Cambois and Stoffa, 1992). The theory of Fourier transform states that any time function $f(t)$ and its frequency spectrum, $F(\omega)$, are related by the Fourier transform, i.e.,

$$F(\omega) = \int_{-\infty}^{\infty} f(t)e^{i\omega t}dt \tag{2}$$

$$f(t) = \frac{1}{2\pi} \int_{-\infty}^{\infty} F(\omega)e^{-i\omega t}d\omega. \tag{3}$$

The equivalence of equation 1 in the Fourier domain is

$$D_{ij}(\omega) = S_i(\omega)R_j(\omega)H_k(\omega)Y_l(\omega). \tag{4}$$

To relate the parameters S, R, H, and Y linearly to the data term D, we take the log of equation 4:

$$\ln\left(D_{ij}(\omega)\right) = \ln\left(S_i(\omega)\right) + \ln\left(R_j(\omega)\right) + \ln\left(H_k(\omega)\right) + \ln\left(Y_l(\omega)\right). \tag{5}$$

Cambois and Stoffa (1992) described in details many of the advantages of the surface-consistent deconvolution in the log/Fourier domain versus the time domain approach by Levin (1989). Some of the advantages mentioned are:

1. the log/Fourier domain is very robust even in the presence of additive noise;

2. the surface-consistent deconvolution becomes linear in this domain; and

3. it separates the signal amplitude and phase into the real and imaginary parts of the complex spectrum.

A review of matching filters

One of the most common practices in digital signal processing is the need to alter the shape of an input signal in order to obtain a desired output (Robinson and Treitel, 1980). This alteration is performed through what's known as shaping or matching filters.

A Matching filter is defined as an operator "which maximizes the output in response to a signal of particular shape" (Sheriff, 1994).

For example, let's consider the problem of finding a filter $f_t = (f_0, f_1, ..., f_m)$ of length $m + 1$ that shapes an input waveform $b_t = (b_0, b_1, ..., b_n)$ of length $n + 1$ into a desired output trace $d_t = (d_0, d_1, ..., d_{m+n})$ of length $m + n + 1$ so that the error between the desired output d_t and the actual output c_t is minimum (Robinson and Treitel, 1980). The actual output is:

$$c_t = \sum_{s=0}^{m} f_s b_{t-s}. \tag{6}$$

This is known as the convolution of the shaping filter with the input signal. The error vector,

$$
\begin{aligned}
\mathbf{e} &= \mathbf{Bf} - \mathbf{d} \\
&= \mathbf{C} - \mathbf{d},
\end{aligned} \tag{7}
$$

where $\mathbf{B}$ is the Topelitz matrix formed from $\mathbf{b}$, $\mathbf{d}$ is a column vector of the desired output trace, and $\mathbf{f}$ is a column vector shaping filter. It's worth noting that our convention in this paper for matrices are upper case boldface and vectors are lower case boldface. Equation 7 is minimized in the least-squares sense by solving the system of the normal equations:

$$
\begin{aligned}
\mathbf{B}^T\mathbf{Bf} &= \mathbf{B}^T\mathbf{d} \\
\mathbf{f} &= (\mathbf{B}^T\mathbf{B})^{-1}\mathbf{B}^T\mathbf{d}
\end{aligned} \tag{8}
$$

The filter coefficients of **f** are given by the cross-correlation of **b** with **d** filtered by the inverse of the autocorrelation of **b**. In matrix form, equation 8 can be written as

$$
\begin{bmatrix}
\phi_0 & \phi_1 & \phi_2 & \phi_3 & . & \phi_m \\
\phi_1 & \phi_0 & \phi_1 & \phi_2 & . & . \\
\phi_2 & \phi_1 & \phi_0 & \phi_1 & \phi_2 & . \\
\phi_3 & \phi_2 & \phi_1 & \phi_0 & \phi_1 & . \\
. & . & . & . & \ddots & . \\
\phi_m & \phi_{m-1} & . & . & . & \phi_0
\end{bmatrix}
\begin{bmatrix}
f_0 \\ f_1 \\ . \\ . \\ \vdots \\ f_m
\end{bmatrix}
=
\begin{bmatrix}
S_0 \\ S_1 \\ . \\ . \\ \vdots \\ S_m
\end{bmatrix},
\tag{9}
$$

where ϕ_m is the mth lag of the autocorrelation of **b** (the input signal) and **s** is the cross-correlation of **b** with **d**.

Implementation of matching filter is relatively simple if two crucial design criteria are met: i) filter length and ii) an optimum lag. Increasing the filter length improves the performance of the matching filters. In practice, as we are going to see later, the maximum it can be is the length of the input signal. The filter lag is considered optimum when signal to noise ratio is high between the input signal and the desired output.

Let's consider matching two signals, **s1** and **s2**. If **m** is a perfect match that converts **s1** into **s2**, which means

$$
\mathbf{m} * \mathbf{s1} = \mathbf{s2}
\tag{10}
$$

where * denotes convolution. In the Fourier domain, equation 10 becomes

$$
M(\omega) = \frac{S_2(\omega)}{S_1(\omega)}.
\tag{11}
$$

Equation 11 means that the Fourier transform of a perfect matching filter is a spectral ratio. It follows that a least-squares match filter, which minimizes $\|\mathbf{S1m} - \mathbf{s2}\|_2$ (L_2 norm), has a Fourier transform which is an approximate match filter.

The least-squares matching filter is preferred because it is stable in the presence of noise while a spectral ratio computed directly is not.

THE THEORY OF SURFACE-CONSISTENT MATCH FILTERING

Extending the surface-consistent data model reviewed previously to the case of designing matching filters to equalize two seismic surveys, we express equation 5 as

$$
\ln\left(D1_{ij}(\omega)\right) = \ln\left(S1_i(\omega)\right) + \ln\left(R1_j(\omega)\right) + \ln\left(H1_k(\omega)\right) + \ln\left(Y1_l(\omega)\right)
\tag{12}
$$

$$
\ln\left(D2_{ij}(\omega)\right) = \ln\left(S2_i(\omega)\right) + \ln\left(R2_j(\omega)\right) + \ln\left(H2_k(\omega)\right) + \ln\left(Y2_l(\omega)\right),
\tag{13}
$$

where indices 1 and 2 used here to denote two data sets, a baseline survey and a monitoring survey (commonly used in time-lapse studies), respectively. Now we write the specral ratio of equations 12 and 13 as follow:

$$
\ln\left(\frac{D2_{ij}(\omega)}{D1_{ij}(\omega)}\right) = \ln\left(\frac{S2_i(\omega)}{S1_i(\omega)}\right) + \ln\left(\frac{R2_j(\omega)}{R1_j(\omega)}\right) + \ln\left(\frac{H2_k(\omega)}{H1_k(\omega)}\right) + \ln\left(\frac{Y2_l(\omega)}{Y1_l(\omega)}\right),
\tag{14}
$$

where the left hand side expresses the trace-to-trace matching filter while the right hand side is its surface-consistent decomposition. Equation 14 linearly relates the unknown parameters $\left(\frac{S2_i(\omega)}{S1_i(\omega)}\right)$, $\left(\frac{R2_j(\omega)}{R1_j(\omega)}\right)$, $\left(\frac{H2_k(\omega)}{H1_k(\omega)}\right)$ and $\left(\frac{Y2_l(\omega)}{Y1_l(\omega)}\right)$ to the known data term $\frac{P2_{ij}(\omega)}{P1_{ij}(\omega)}$. Determining these unknowns form the solution to our problem, the surface-consistent matching filters.

In the seismic world, this problem is known to have both overdetermined (there are more data than unknowns) and underconstrained (solutions are nonunique) form, similar to the statics problem analyzed by Wiggins et al. (1976).

In order to solve this problem as a general linear inverse problem, equation 14 is simplified to its matrix form

$$\mathbf{d} = \mathbf{Gx} \tag{15}$$

where

$$\mathbf{x} = \begin{bmatrix} \mathbf{s} \\ \mathbf{r} \\ \mathbf{h} \\ \mathbf{y} \end{bmatrix},$$

$$S_i = \ln\left(\frac{S2_i(\omega)}{S1_i(\omega)}\right), R_j = \ln\left(\frac{R2_j(\omega)}{R1_j(\omega)}\right), H_k = \ln\left(\frac{H2_k(\omega)}{H1_k(\omega)}\right), Y_l = \ln\left(\frac{Y2_l(\omega)}{Y1_l(\omega)}\right), \text{and}$$

$$\mathrm{D}_{ij} = \ln\left(\frac{D2_{ij}(\omega)}{D1_{ij}(\omega)}\right).$$

However, practically taking the ratio of two spectra proved to be numerically impossible for at least two reasons:

1. a spectrum can have zero values and therefore it becomes an unstable division; and

2. theoretically, obtaining a matching filter through straight division (if it were possible) results in an exact match of the data but the consequences are amplification of noise.

Alternatively, we designed a matching filter, $\mathbf{m}$, in the time domain so that two seismic traces are matched in a least-squares sense:

$$\mathbf{d1} = \mathbf{D2m}, \tag{16}$$

where $\mathbf{d1}$ and $\mathbf{d2}$ represent the same trace from survey 1 and 2, respectively. $\mathbf{D2}$ is a convolution matrix formed from $\mathbf{d2}$. Cross-correlation between the two traces is required to determine the lag time. This time shift is employed in the convolution with trace $\mathbf{d1}$.

To solve equation 16 is to find $\mathbf{m}$ such that the L_2 norm, $\|\mathbf{d1} - \mathbf{D2m}\|_2$, is minimum. Several methods in linear inverse theory are available but we employed the normal equation method of solution:

$$\mathbf{m} = (\mathbf{D2}^T\mathbf{D2} + \alpha^2\mathbf{I})^{-1}\mathbf{D2}^T\mathbf{d1}, \tag{17}$$

where α is a stabilization factor.

Once a matching filter is determined between each trace of survey $\mathbf{d1}$ and its equivalent in

survey **d2**, we transform the result into the frequency domain then we take the log of the complex spectrum. We store the log of the complex spectrum inside a data matrix that has a special arrangement, where in the rows we have $d_{1,1},...,d_{1,nr},d_{2,1},...,d_{2,nr}$, ...etc. The first index denotes the shot number and the second denotes the trace number. In total we have $N_S * N_T$ data.

Using the inverse of the geometry matrix, **G**, we can now decompose **p**, which is a vector containing one frequency from all of the **m**'s in equation 17 for the entire survey,into four components:

$$\mathbf{x} = (\mathbf{G}^T\mathbf{G} + \alpha^2\mathbf{I})^{-1}\mathbf{G}^T\mathbf{p}. \tag{18}$$

G contains the positions of the four-components in equation 15. The unknown parameters themselves are ordered (**s**, **r**, **h**, and **y**) in the vector **x**. The geometry matrix **G** relates the unknown parameters **x** to the data vector **d**. Understanding the construction of the geometry matrix **G** is key to obtaining an accurate surface-consistent matching filter. In the next section, we will show how **G** is constructed for a symbol 2D synthetic seismic line.

APPLICATION TO SYNTHETIC DATA

To apply equation 15, the following elements are required:

1. two seismic surveys resampled to a common grid to compensate for differences in acquisition geometries;

2. a geometry matrix that contains the positions of the source, receiver, offset, and midpoint; and

3. knowledge about the static and dynamic part of the data to help design the matching filters length.

A complete description of the acquisition of the synthetic data is provided below as well as the construction of the geometry matrix and how it is being inverted. Two examples are presented to demonstrate what each of the surface-consistent matching filters contains and how to apply them.

Synthetic dataset

The earth model constructed for this experiment is a simple 2.5km wide and 1km thick 2D geometry (Figure 1). The model consists of four layers and a reservoir unit, 500m wide and 20m thick, between layers three and four. The velocity is homogeneous in each layer except for the near surface layer where lateral variations were introduced. Using this geologic structure, we generated three velocity models, a baseline, a first monitoring and a second monitoring. The subsurface of the baseline model and the first monitoring model is exactly the same. The near-surface layer has different velocity and different attenuation for both models. In the first monitoring model, this layer has a 20% increase in velocity but less attenuation compared to the baseline model. The third model, the second monitoring, has similar properties to the first monitoring except the reservoir layer velocity is different.

The velocity of the reservoir layer in the second monitoring model is higher by about 10% ($\sim 350m/s$). There are 26 shots with spacing of a $100m$ and 101 receivers per shot with a spacing of $10m$ (Figure 2). The maximum record length is $1s$ with a $4ms$ sampling interval. An acoustic finite difference algorithm is used to generate three seismic surveys (a baseline, a first monitoring and a second monitoring). We used a minimum phase wavelet with a dominant source frequency of $20Hz$. In addition to the variations of velocity in the geologic model, source strength and receiver coupling are made variable for all surveys.

Constructing and inverting the geometry matrix G

The structure of the geometry matrix, **G**, for the 2D seismic line discussed above, is illustrated in Figure 3 where the nonzero entries in the columns indicate the position of the sources, the receivers, the offsets and the midpoints. The number of nonzero entries in any corresponding column represent the equation redundancy for that term (Wiggins et al., 1976). For example, the nonzero entries in the shot columns indicate the equation redundancy for the shot terms equal to the number of receivers per shot. Similarly, the offset terms have a redundancy of half the number of receivers per shot. The receiver terms and the structural terms show less redundancy in comparison. Computing the total number of unknown parameters, N_P, for this example is relatively easy. The total number of shots are denoted by N_S and the total number of traces per shot are denoted by N_T. The shot spacing differs from the receiver spacing, hence the following computations have to be modified for different geometries:

$$
\begin{aligned}
N_R &= 2(N_T + N_S) - 1 \\
N_Y &= 2N_R - 1 \\
&= 4(N_T + N_S) - 3 \\
N_H &= N_T \\
N_D &= N_S * N_T \\
N_P &= N_S + N_R + N_Y + N_H \\
&= 7N_S + 7N_T - 5
\end{aligned}
$$

where

N_R is the total number of unique receiver positions;

N_Y is the total number of unique offset positions;

N_H is the total number of unique midpoint positions;

N_D is the total number of data; and

N_P is the total number of unknown parameters.

To solve equation 15 is to find the best least-squares solution that minimizes the L_2 norm of the residual, $\|\mathbf{d} - \mathbf{Gx}\|_2$, which corresponds to solving the system of normal equations:

$$
\mathbf{x} = (\mathbf{G}^T\mathbf{G})^{-1}\mathbf{G}^T\mathbf{d}.
$$

The square matrix $\mathbf{G}^T\mathbf{G}$ is singular and therefore no unique inverse exists (Figure 4). Nevertheless, the general inverse theory allows us to solve for the determined terms. There are several ways to solving an overdetermined system but we only attempted two methods which gave similar result. The first is by using the singular value decompositioning (SVD), also known as the Moore-Penrose pseudoinverse, to compute an inverse for $\mathbf{G}$:

$$\mathbf{G}^\dagger = \mathbf{V}_p\mathbf{S}_p^{-1}\mathbf{U}_p^T,$$

where $\mathbf{V}_p$, $\mathbf{S}_p$ and $\mathbf{U}_p$ represent the nonzero components of the SVD of $\mathbf{G}$. In MATLAB, a **pinv** command solves for $\mathbf{G}^\dagger$ with a tolerance option such that no singular values below the tolerance are invertible. The other method of inversion used is the normal equations:

$$(\mathbf{G}^T\mathbf{G} + \alpha^2\mathbf{I})^{-1}\mathbf{G}^T,$$

where $\mathbf{I}$ is the identity matrix and α is the tolerance factor mentioned above. In this study, we experimented with many tolerance numbers and found that 1 was a suitable one to use and therefore all singular values below 1 are not included in the inversion.

Applying the match filters

Using the three synthetic models built for this study (baseline, first monitoring, and second monitoring) we discuss how the surface-consistent matching filters are applied. Two matching filters are computed. The first is between the baseline survey and the first monitoring survey. The other filter is between first monitoring survey and second monitoring survey.

Figure 5 illustrates the four-components surface-consistent matching filters computed from the first example. The assumption of the surface-consistent model is that the shot-consistent components collects the effects of the source signature and the near-surface effects imposed on the downgoing source waveform. Similarly, the receiver-consistent components are assumed to collect the effects of the receiver response and the near-surface influence around each receiver on the recorded waveform.

A quantitative assessment of the decomposition of the source- and receiver-consistent components is illustrated in Figure 6. Only in experimental work could this assessment be possible since the input source strengths and receiver couplings are known. The ratio of the input source strengths compared to the predicted source strengths are evidence that source-consistent components separate the influence on the recorded waveform due to source signature. Likewise, the ratio of the input receiver coupling compared to the predicted receiver coupling are similar which is evidence that the receiver-consistent components separate the influence on the recorded waveform due to receiver response.

Figure 5 also illustrates the offset and midpoint components. We notice an interesting feature on the offset-consistent term between $430m$ and $500m$. This feature is due to the first break event being included at these far-offsets inside the window of the match filter. Although this probably will not occur in a real data set, it still interesting that the offset-components collect such effects and we desired to keep it in the filter window without using the power of muting.

Previous studies, such as Cary and Lorentz (1993) and Levin (1989), have reported that ground roll and other coherent noise effects are collected in the offset-components. Apparent increase in frequency with offset was reported to being visible on the offset-component by Cary and Lorentz (1993) which they attribute it to differential normal moveout.

For the case of the midpoint component, it is known to be effective in collecting the subsurface effects. It also collects noise and hence smoothing is highly recommended to overcome the noise. In this study, we choose not to smooth the midpoint component but we plan to examine it in the future.

Figure 7 shows our first example, that is matching the first monitoring survey to the baseline survey. The differences between these two models are in the near-surface only and their subsurfaces are unchanged. The computed surface-consistent matching filters are applied to the first monitoring survey and a matched survey (or predicted survey) is produced.

Figure 8 illustrates our second example where we have introduced some variations in the subsurface reservoir properties in second monitoring but both first and second monitoring have the same near-surface model. We have also accounted for differences in acquisition instruments by introducing differences in source strengths and receiver couplings between the two surveys. The computed surface-consistent matching filters are applied to second monitoring survey and a predicted survey is produced.

After several trials, we decide that the length of the matching filters of $0.3s$ centered around the middle reflector (Figures 7 and 8) provide a better result. It is common to use a short operator that is similar in length to the two wavelets being matched. The idea is to provide a close enough spectral and phase match to compensate for differences in amplitudes and time-shifts between the two surveys and avoid an overmatch that can zero-out actual differences caused by petrophysical changes in the dynamic section of the subsurface (Lumley, 1995).

DISCUSSION

Figure 7 shows an example of a baseline and a first monitoring shot record from which the matching filter components in Figure 5 were computed. Our goal is to match the first monitoring survey to the baseline survey. The result shown in Figure 7c (predicted survey) is the convolution of the matching filter components with the first monitoring survey. The difference between the baseline survey and the predicted survey in the window where the matching filter is applied is extremely small. Note, all the seismic panels in Figure 7 have the same amplitude scaling.

The second example is presented in Figure 8 where we attempt to match second monitoring survey to first monitoring survey. The residual between first monitoring and the predicted survey is almost zero in the window where the matching filter is applied. Below the window of the matching filter, we observe the continuous coherent event that is due to the changes in the reservoir. It is important to recall that both surveys have the same near-surface model but their subsurface model, the receiver couplings and source strengths are different. The issue in this example, as one might expect, is mainly amplitude differences

and the computed surface-consistent matching filters proved to have compensated for this problem.

To quantify the success of the surface-consistent matching filters, visual aids are not enough. A common measure of differences in time-lapse processing is normalized rms (nrms) within a time window in the static section of the seismic. Nrms is considered as the metric system that measures the repeatability between two traces a_t and b_t in a time gate (Kragh and Christie, 2002):

$$NRMS = 2\frac{RMS(a_t - b_t)}{RMS(a_t) + RMS(b_t)}. \tag{19}$$

It is often the case that nrms values are expressed as a percentage. The nrms values are not intuitive and are not limited to 0 - 100%. As described by Kragh and Christie (2002), if both a_t and b_t contain random noise, the nrms value is 141%. If both traces anticorrelate the nrms value is 200%, and if one trace is half the amplitude of the other the nrms value is 67%. To summarize, low nrms values indicate higher similarity between traces.

We see in Figure 9 that trace #40 from the baseline survey (in Figure 7) correlates well with the same trace from the first monitoring survey. This good correlation translates into a low nrms value (18 %) shown in Figure 10 at x-coordinate 1290m. Similarities in amplitude spectra, such as that shown in Figure 10 for trace #40, particularly in the low frequency range will tend to result in low nrms values. On the contrary, trace #86 shown in Figure 10b illustrates that the matching filters performance is not optimum, hence the residual seen at this trace's location in Figure 9d. The nrms value for this trace (x-coordinate 1750m) is 50%. Unlike trace #40, the amplitude spectra for trace #86 show dissimilarities at low frequency range.

In the second data sets, because traces from first monitoring survey correlates well with traces from second monitoring survey, as shown in Figure 11, the nrms values in Figure 12 are pleasingly low (max at about 2.5%). In general, there is a high correlation in the amplitude spectra of the two surveys particularly over low to mid frequency range (Figure 12b and c).

CONCLUSIONS

In conclusion, we have demonstrated that theoretically a surface-consistent matching filter that is useful for processing time-lapse seismic data is possible. This hypothesis is analogous to the well known four-component surface-consistent deconvolution except that it considers two repeated seismic surveys instead of just one.

We constructed three geologic models and used CREWES finite difference algorithm to acquire seismic data sets. Two matching operators were computed in the time domain in the least-squares arithmetic. In the first example, we applied all four-components to the first monitoring survey to match it to the baseline survey whose subsurface (the reservoir) is unchanging but which show surface-consistent variability. The result is then Fourier transformed providing us with the data term in frequency domain. We decomposed the data term into its surface-consistent components: source, receiver, offset, and midpoint.

We discussed what each of these components collects and utilized all four-components to equalize the first monitoring survey to the baseline survey. We claimed that the residual is very small as shown in difference plots and with the support of the nrms we illustrated that in general the matching filters reduced the residuals quite significantly. Such satisfying results were obtained despite the fact that we realized later in our work that our near-surface model was more complicated than what a real geologic model might be. The difficulties arise from introducing lateral velocity variations every $1m$.

In the second example, the objective was to compute a filter that match the second monitoring survey and the first monitoring survey where both surveys exhibited variable reservoir and showed surface-consistent variability as well. In this case, the residual is close to zero in the calculated matching filter window.

The results of this work are encouraging. We also have listed several tasks that need to be worked on in order to examine nrms behavior and to examine the matching filters capability to equalize two data sets. These tasks include stacking the shot records of the predicted data and that of the baseline data and evaluate the difference. We also plan to examine the effects of reducing the offset terms and/or the midpoint terms on the matching filters. Finally, we look forward to applying this new algorithm on a real time-lapse data set and explore some of the challenges present in real examples.
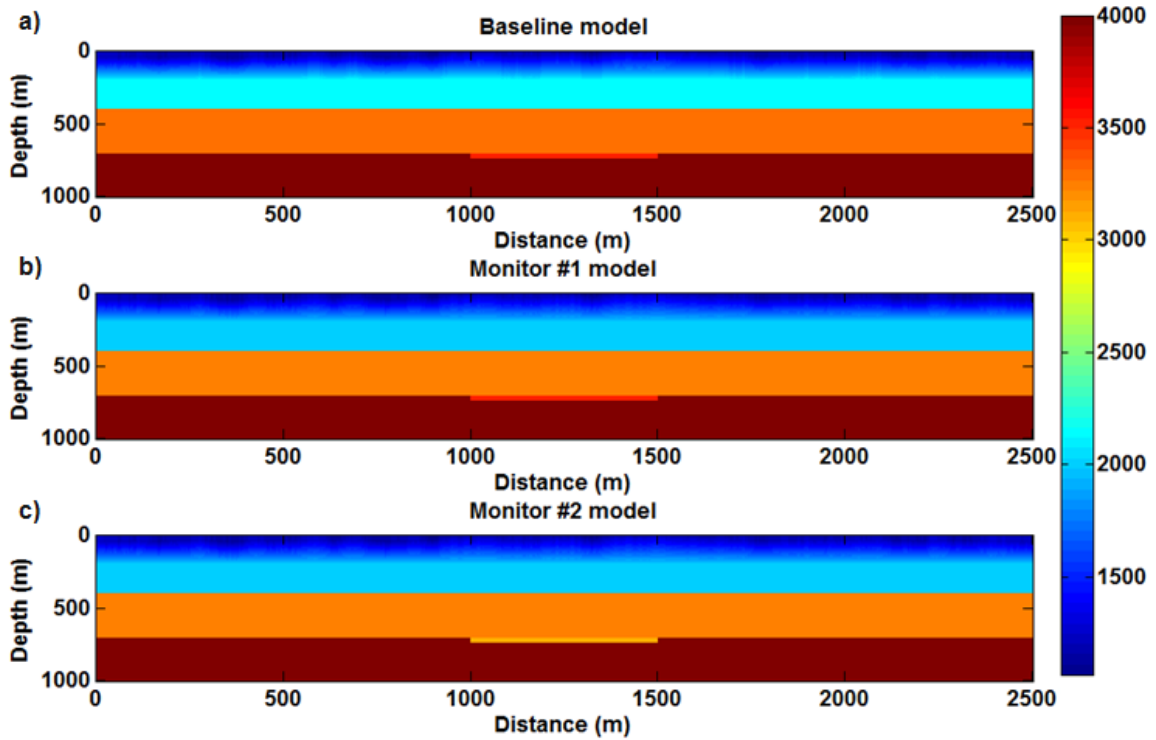
FIG. 1: Three velocity models for (a) baseline survey, (b) first monitoring survey and (c) second monitoring survey.
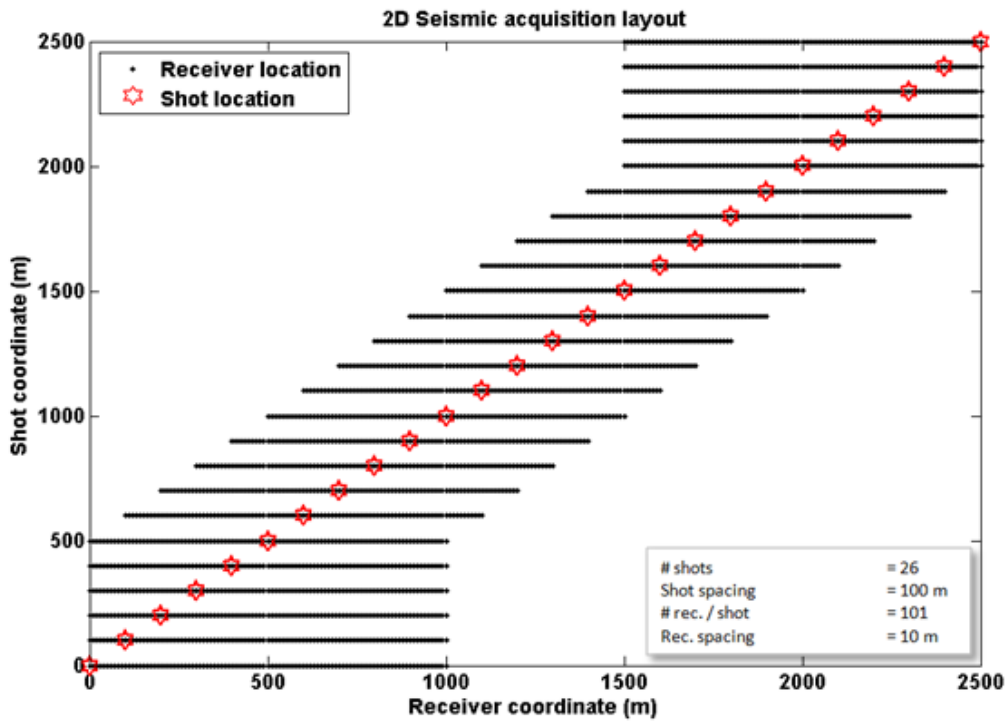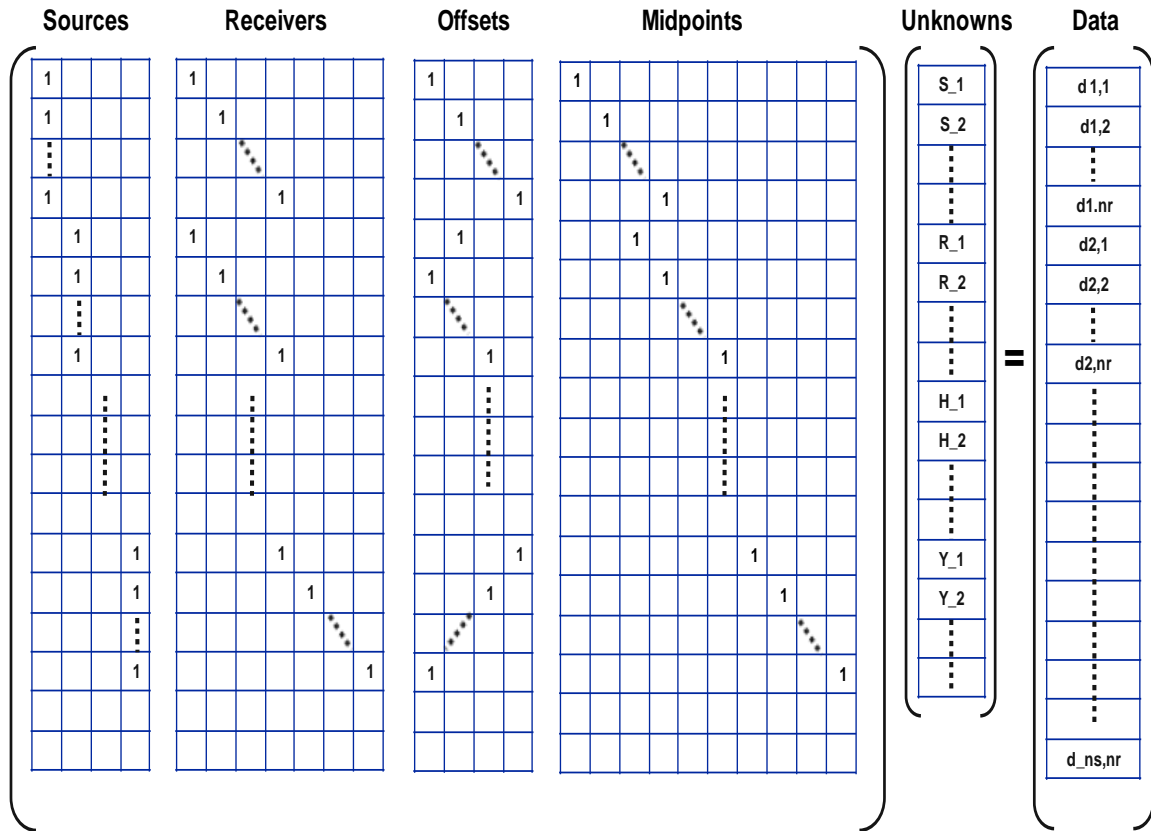

FIG. 2: Acquisition geometry.

FIG. 3: Matrix structure of the system of linear equation described in equation 15.
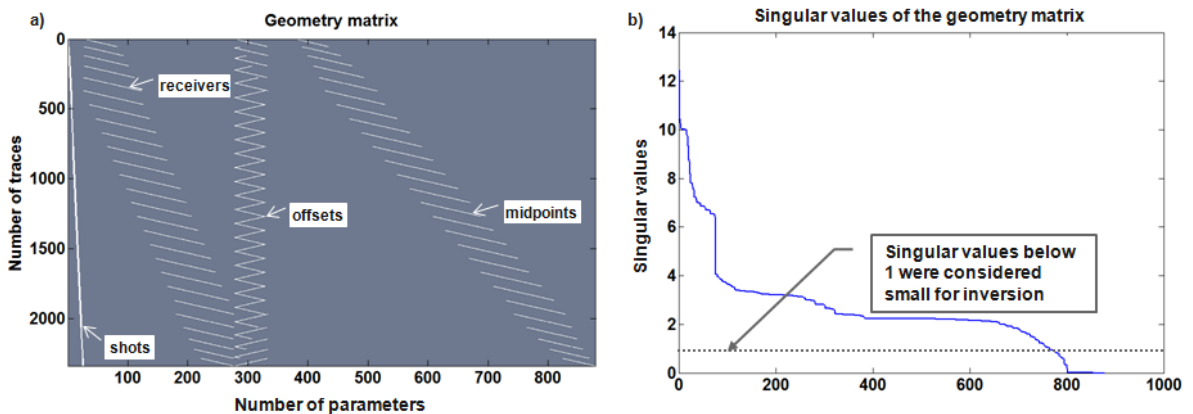

FIG. 4: Data geometry structure shown in (a) and the singular values of the geometry matrix in (b).
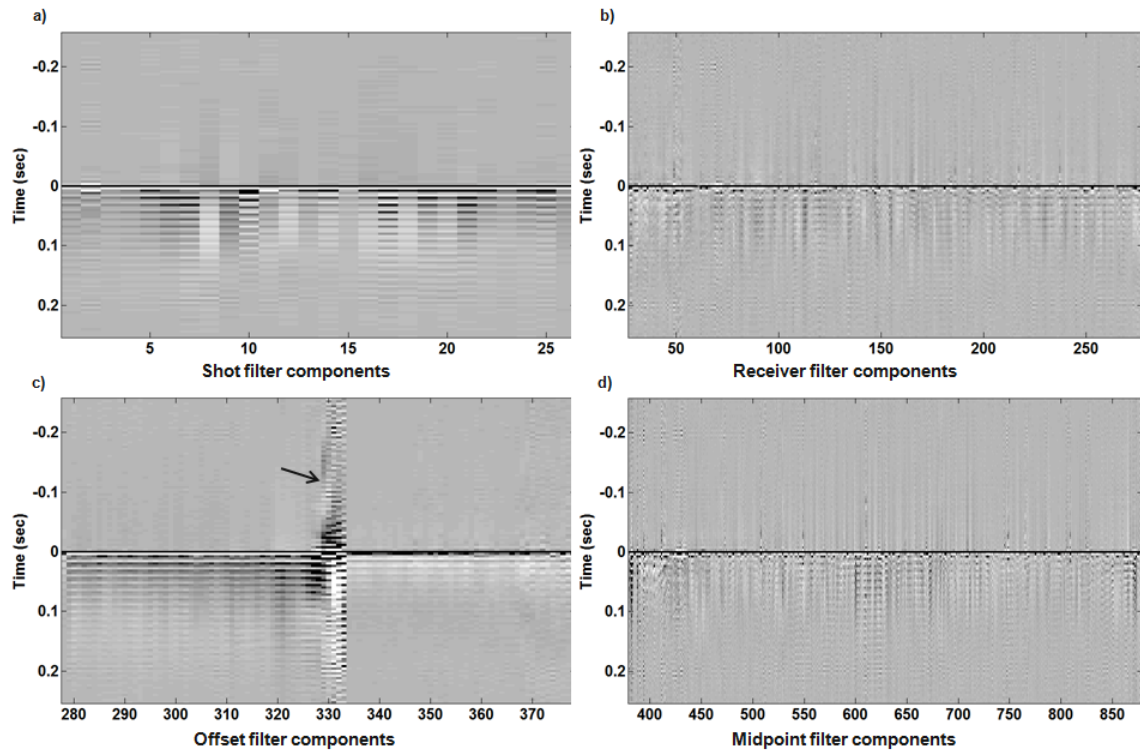
FIG. 5: The four-components surface-consistent matching filters computed from the baseline survey and the first monitoring survey. Panels (a-d) show the shot filter components, receiver filter components, offset filter components, and midpoint filter components, respectively. Note in the offset filters there is an increased level of noise related to first break arrivals included, at far-offsets (430-500m), inside the operator window as illustrated in Figure 7a.
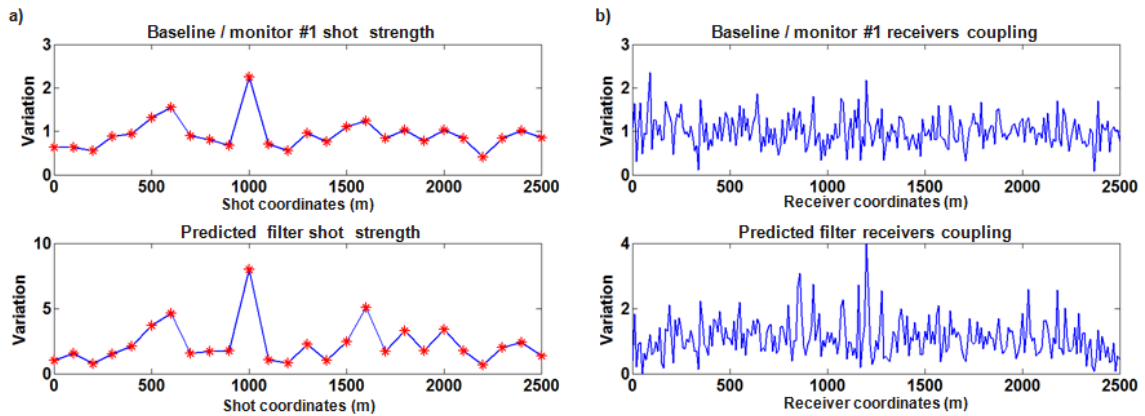
FIG. 6: Input source strengths (a) compared to predicted source strengths (b). Similarly, the input receiver couplings (c) compared with the predicted receiver couplings (d).
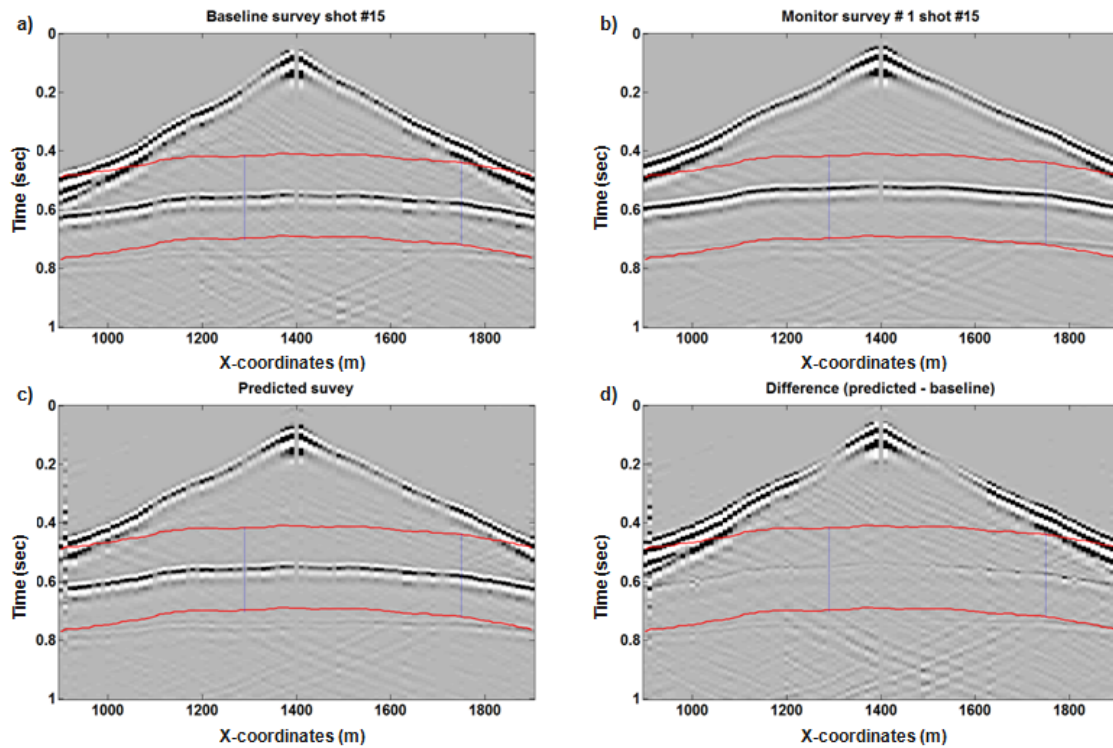
FIG. 7: Shot gather #15 from the 2D seismic line acquired over the synthetic model. Panels (a-b) are the baseline survey and the first monitoring survey, respectively. The predicted survey, convolution of fist monitoring with the matching filters in Figure 5, is shown in (c). The difference between the predicted data and the baseline data is in (d). The two red lines represent the window of the computed matching filters.
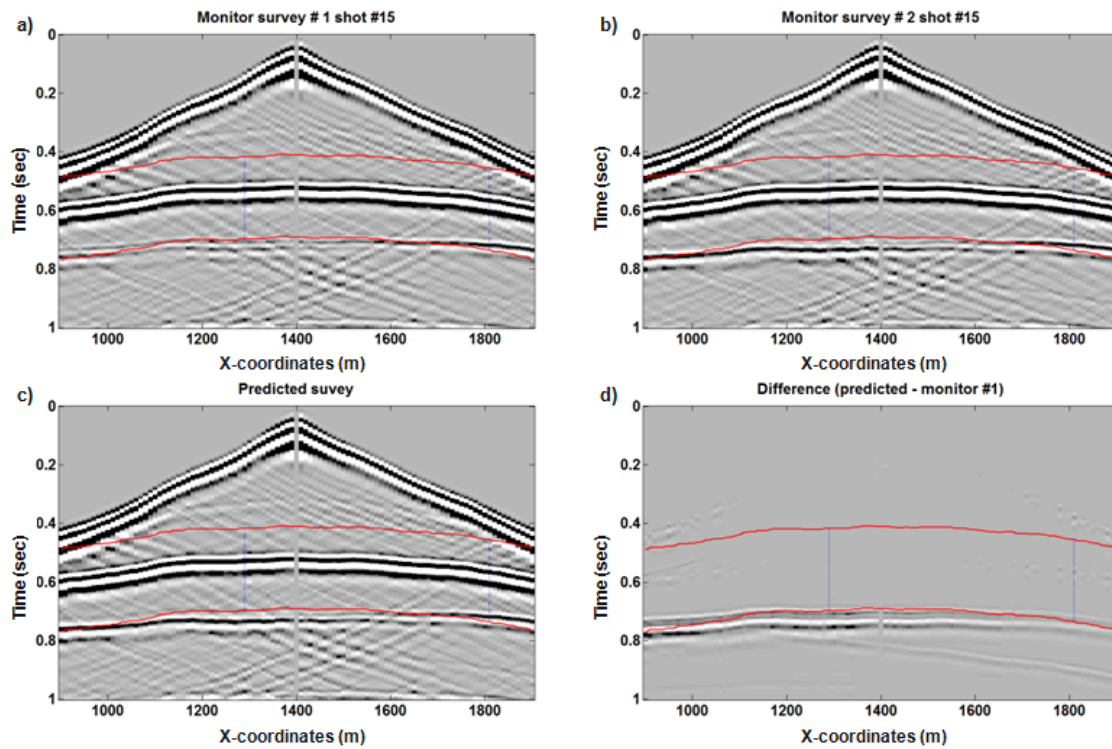
FIG. 8: Shot gather #15 from the 2D seismic line acquired over the synthetic model. Panels (a-b) are the first monitoring survey and the second monitoring survey, respectively. The predicted survey, convolution of second monitoring with the matching filters, is shown in (c). The difference between the predicted data and the first monitoring data is in (d). The two red lines represent the window of the computed matching filters.
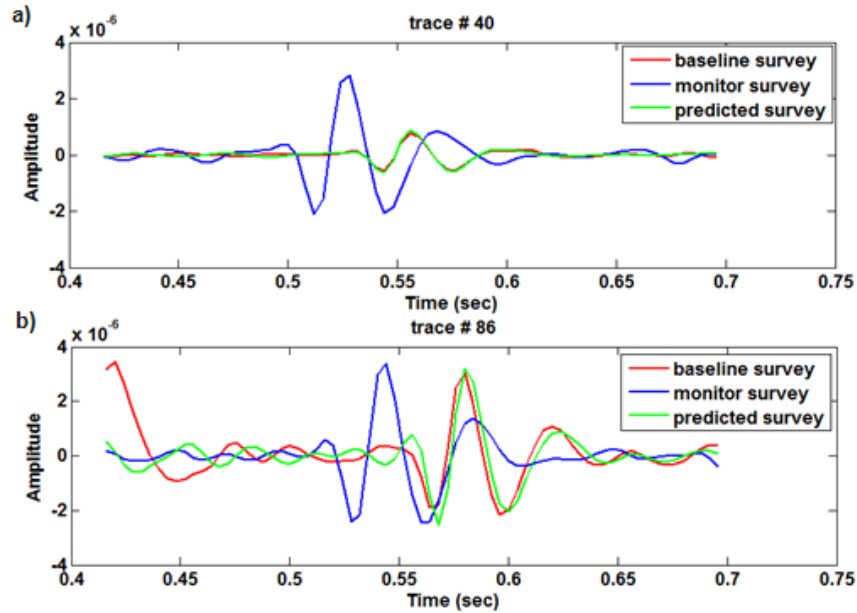
FIG. 9: (a) Trace 40 extracted from the baseline, the first monitoring, and the predicted data (left blue line in Figure 7). This trace shows an excellent match between the predicted and the baseline data. (b) Shows trace 86 where a small difference is exhibited between the predicted data and the baseline data.
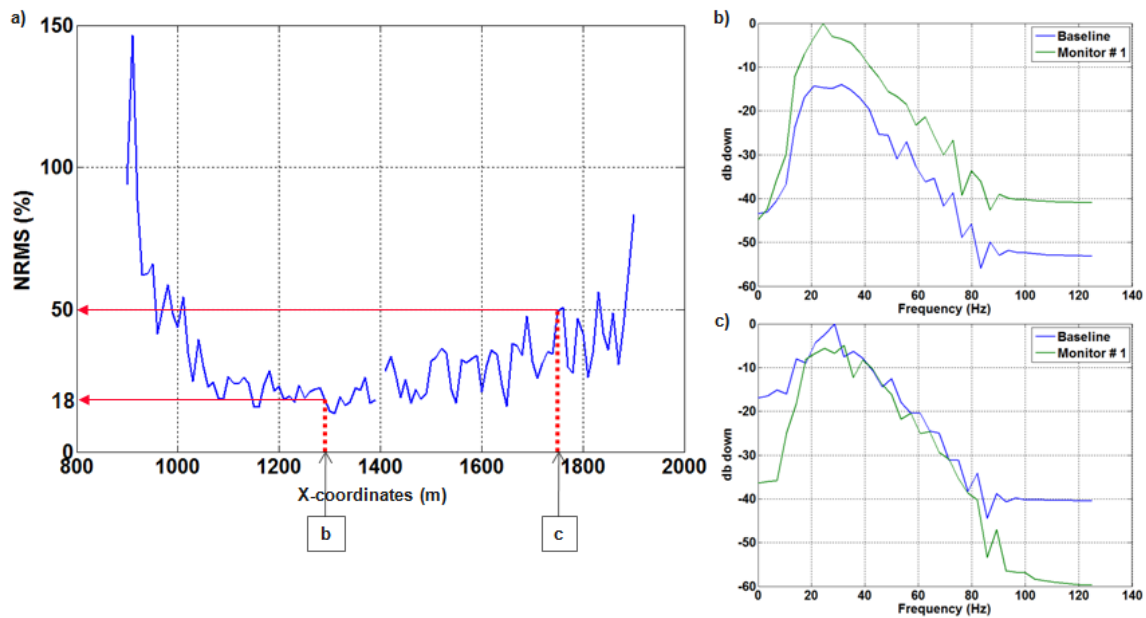

FIG. 10: (a)The nrms as computed by equation 19 between the baseline survey and the first monitoring survey. Traces on the both ends of the shot #15 display high degree of anticorrelation, whereas traces in the middle have low nrms values , hence relatively good match. Panels (b-c) illustrate amplitude spectra of trace 40 and trace 86, respectively, from the baseline and the first monitoring data. Note when amplitude spectra of both data set is different in low frequency ranges, as in (c), the match will tend to be poor.
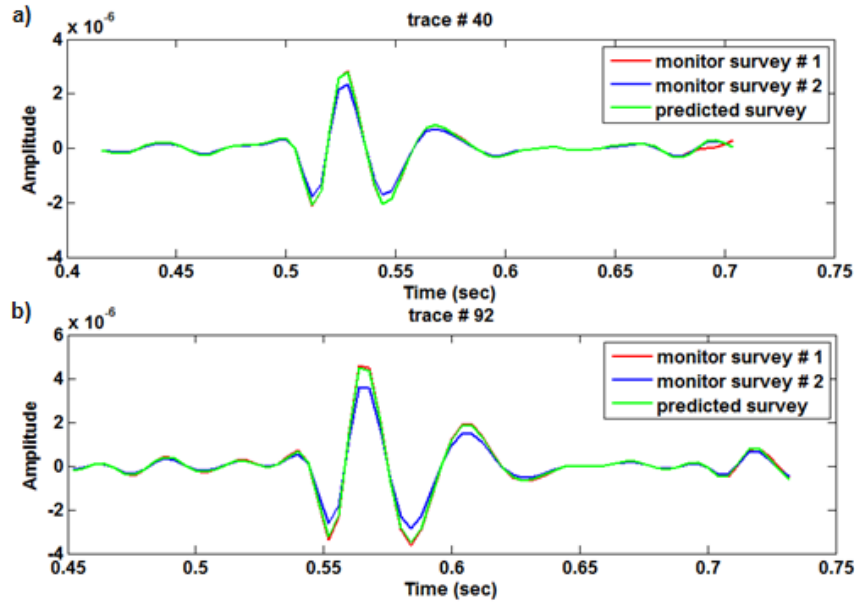
FIG. 11: (a) Trace 40 extracted from the first monitoring, the second monitoring, and the predicted data (left blue line in Figure 8). This trace shows an excellent match between the predicted and the baseline data. (b) Shows trace 92 with excellent match between the predicted data and the first monitoring.
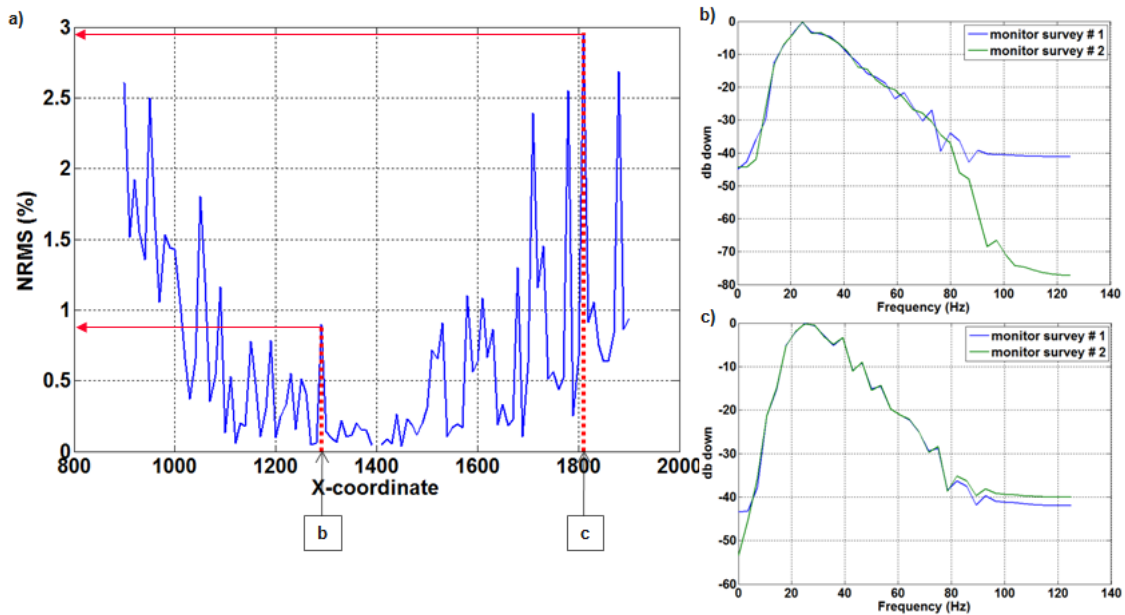

FIG. 12: (a) Nrms computed between first monitoring survey and second monitor survey. Successful match between the two surveys is demonstrated by the very low nrms values. Panels (b-c) illustrate amplitude spectra of trace 40 and trace 92, respectively, from the first monitoring and the second monitoring data where both data set display similar amplitude spectra.

REFERENCES

Almutlaq, M. and Margrave, G. F. (2010). Towards a surface consistent match filter (scmf)for time-lapse processing. *CREWES Research Report*, (22).

Cambois, G. and Stoffa, P. L. (1992). Surface-consistent deconvolution in the log/fourier domain. *Geophysics*, (57):823–840.

Cary, P. W. and Lorentz, G. A. (1993). Four-component surface consistent deconvolution. *Geophysics*, (58):383–392.

Jack, I. (1998). Time-lapse seismic in reservoir management. *SEG short course notes*.

Kragh, E. and Christie, P. (2002). Seismic repeatability, normalized rms, and predictability. *TLE*, (7):640–647.

Levin, S. A. (1989). Surface-consistent deconvolution. *Geophysics*, (54):1123–1133.

Lumley, D. E. (1995). Seismic time-lapse monitoring of subsurface fluid flow. *PhD thesis, Stanford Univ.*

Morley, L. and Claerbout, J. (1983). Predictive deconvolution in shot-receiver space. *Geophysics*, (48):515–531.

Robinson, E. A. and Treitel, S. (1980). Geophysical signal analysis. *Prentice-Hall, Inc.*

Sheriff, R. E. (1994). Encyclopedic dictionary of exploration geophysics. *SEG*.

Taner, M. T. and Coburn, K. W. (1980). Surface consistent estimation of source and receiver response functions. *50th Annual International SEG Meeting*.

Taner, M. T. and Koehler, F. (1981). Surface consistent corrections. *Geophysics*, (46):17–22.

Taner, M. T., Koehler, F., and Alhilali, K. A. (1974). Estimation and correction of near-surface time anomalies. *Geophysics*, (39):441–463.

Taner, M. T., Lee, L., and Baysal, E. (1991). Static corrections: time, amplitude, and phase. *SEG Exp. Abst.*

Wiggins, R. A., Larner, K. L., and Wisecup, R. D. (1976). Residual static analysis as a general linear inverse problem. *Geophysics*, (41):922–938.

Yu, G. (1985). Offset-amplitude variation and controlled-amplitude processing. *Geophysics*, (50):2697–2708.